ACS APPLIED MATERIALS & INTERFACES

Research Article

www.acsami.org

Tailoring Nucleation at Two Interfaces Enables Single Crystalline NiO Nanowires via Vapor−Liquid−Solid Route

Kazuki Nagashima,[†] Hideto Yoshida,[‡] Annop Klamchuen,[§] Masaki Kanai,[†] Gang Meng,[†] Fuwei Zhuge,[†] Yong He,[†] Hiroshi Anzai,[†] Zetao Zhu,[†] Masaru Suzuki,[†] Mickaël Boudot,[†] Seiji Takeda,[‡] and Takeshi Yanagida*[,†]

[†]The Institute for Materials Chemistry and Engineering, Kyushu University, 6-1 Kasuga-Koen, Kasuga, Fukuoka 816-8580, Japan

[‡]The Institute of Scientific and Industrial Research, Osaka University, 8-1 Mihogaoka Ibaraki, Osaka 567-0047, Japan

[§]National Nanotechnology Center (NANOTEC), NSTDA, 111 Thailand Science Park, Pathumthani 12120, Thailand

ABSTRACT: Here we show a rational strategy to fabricate single crystalline NiO nanowires via a vapor−liquid−solid (VLS) route, which essentially allows us to tailor the diameter and the spatial position. Our strategy is based on the suppression of the nucleation at vapor−solid (VS) interface, which promotes nucleation only at the liquid−solid (LS) interface. Manipulating both the supplied material fluxes (oxygen and metal) and the growth temperature enables enhancement of the nucleation only at the LS interface. Furthermore, this strategy allows us to reduce the growth temperature of single crystalline NiO nanowires down to 550 °C, which is the lowest growth temperature so far reported.

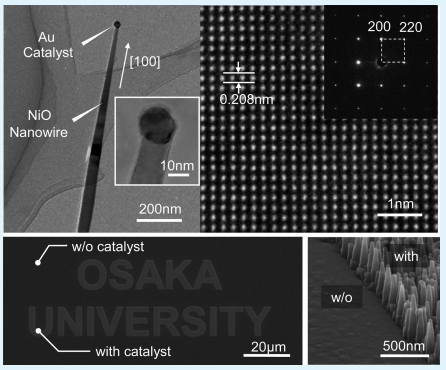

KEYWORDS: *nickel oxide nanowire, vapor−solid−liquid process, vapor flux control, single crystalline oxide nanowire, memristive switching*

1. INTRODUCTION

Nickel oxide (NiO), which is a simple binary metal oxide with the rock-salt crystal structure, is an attractive functional material due to its fascinating fundamental physical properties, such as antiferromagnetism, p-type semiconductivity, catalytic properties, and others,[1−4] and also their diverse device applications, including the use as a supercapacitor,[5,6] nonvolatile memory,[7−10] lithium ion battery,[11,12] and solar cell.[13,14] Among various nanostructures of NiO, single crystalline NiO nanowires are promising because of the applicability to fundamentally study nanoscale physical properties of NiO[15] and also NiO-based functional nanodevices by utilizing the well-defined and tailorable surface properties with the large area.[16,17] Although there are various methods to form NiO nanowires,[18−31] the so-called vapor−liquid−solid (VLS) process with metal catalysts offers a promising way to fabricate single crystalline NiO nanowires because the VLS process allows us to tailor the diameter, the spatial position, and the heterostructures of nanowires, which are not attainable by other nanowire growth methods.[32−39] However, the VLS nanowire growth of NiO has been substantially limited and difficult due to the lack of understanding of the fundamental process of VLS growth for NiO. One of possible reasons for this difficulty might be the relatively low vapor pressure of Ni (5.97×10^{-8} Pa at 850 °C), which is substantially lower (at least 4 orders up to 12 orders) than those of metals, whose oxide nanowires are easily formed via VLS route (for example, Zn, 6.12×10^{4} Pa; Mg, 8.87×10^{3} Pa; In, 2.82×10^{-1} Pa; Sn, 4.14×10^{-4} Pa at 850 °C).[40,41] This low vapor pressure of Ni might hinder the nanowire growth of NiO via VLS route at conventional growth temperatures (up to 800 °C) because the nucleation at the vapor−solid (VS) interface must be enhanced for such low vapor pressure materials, which is detrimental for VLS process. The straightforward approach to overcome this issue might be the use of a higher growth temperature (for example higher than 1000 °C) to suppress the nucleation at the VS interface and also enhance the nucleation only at the LS interface for the VLS process.[27,28] However, such a high temperature process strongly limits the application range due to the integrations with other processes and materials. Therefore, a realization of the VLS process for NiO at a relatively low temperature range is desired. Here, we propose a rational strategy to fabricate a single crystalline NiO nanowire via the VLS route by tailoring a nucleation at both VS and LS interfaces. This strategy is based on the so-called "material flux window" principle.[42,43] Manipulating both the supplied material fluxes (oxygen and metal) and the growth temperature enables us to enhance the nucleation only at the LS interface. Furthermore, this strategy allows us to reduce the growth temperature of single crystalline

Received: August 4, 2016
Accepted: September 27, 2016
Published: September 27, 2016

DOI: 10.1021/acsami.6b09761
ACS Appl. Mater. Interfaces 2016, 8, 27892−27899

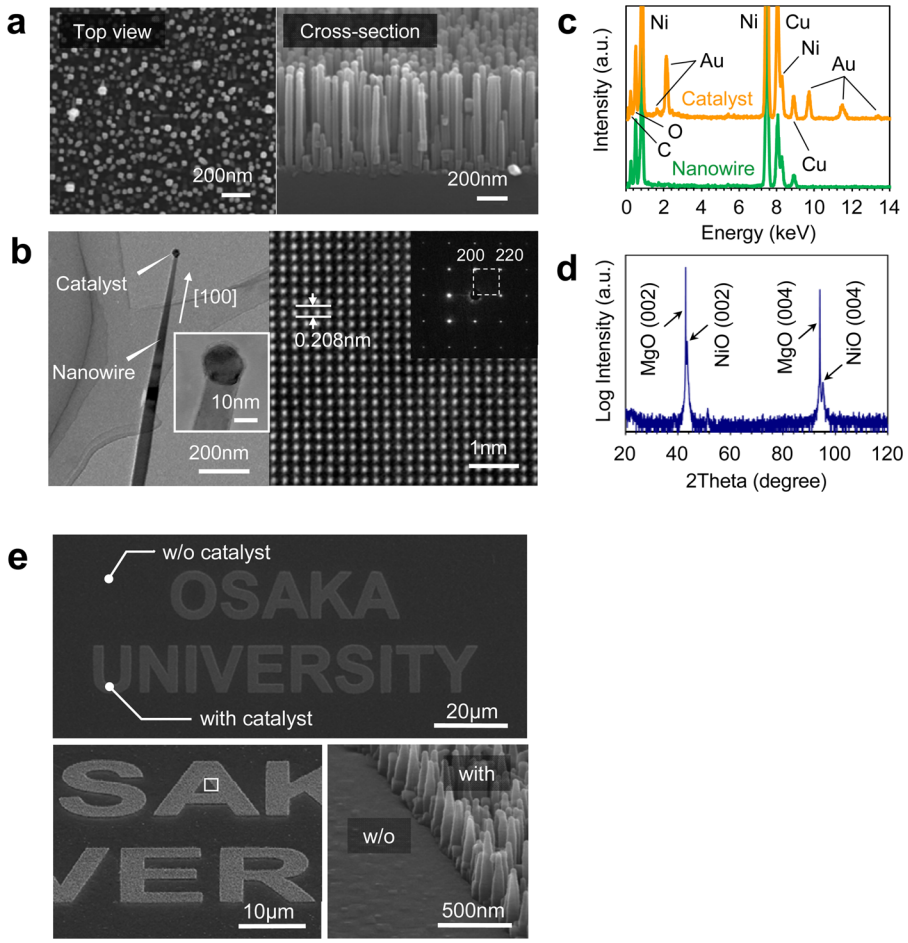

Figure 1. (a) FESEM images of NiO nanowires grown onto a MgO(100) single crystalline substrate. The growth temperature, the Ni flux, and the oxygen partial pressure were 850 °C, 1.8 × 10^{18} atoms/cm^2 s, and 10^{-3} Pa, respectively. The left part shows a top view image, and the right part shows a cross-sectional image. (b) TEM images of NiO nanowires. The left part shows an overview image of a NiO nanowire. Inset in the left part is a magnified image around the catalyst at the tip of NiO nanowire. The right part shows a high resolution TEM image of a NiO nanowire. Inset in the right part is an SAED pattern, indicating the single crystal nature and cubic structure of NiO nanowire. (c) EDS spectra of a NiO nanowire taken at near the catalyst (yellow) and the nanowire body (green). (d) XRD pattern of NiO nanowires on MgO substrate. (e) Spatial selectivity of present NiO nanowires.

NiO nanowires via the VLS route down to 550 °C, which is the lowest growth temperature so far reported.[27,28]

2. EXPERIMENTAL SECTION

For the NiO nanowire growth, we utilized the pulsed laser deposition (PLD) technique using an ArF excimer laser (Lamda-Physik, COMPex 102, λ = 193 nm).[32−35] Prior to the nanowire growth, ∼1 nm thick Au, which was used as catalyst for nanowire growth, was deposited onto a MgO (100) single crystal substrate by dc sputtering (SANYU Electron, SC701-HMC). The background pressure was ca. 1 × 10^{-5} Pa. Then, the O_2/Ar mixture gas was introduced into the chamber with varying oxygen partial pressures from 10^{-5} to 10 Pa by maintaining 10 Pa of the total pressure. The substrate temperature was raised up to the objective value within 20 min before the deposition. The vapor source was supplied by ablating the NiO tablet (99.9% pure). To control the vapor flux, the laser energy and the substrate−tablet distance were varied in the ranges 40−80 mJ and 30−45 mm, respectively. In addition, the attenuator was introduced to further control the vapor flux at a small flux range. The Ni flux with units of atom/cm^2 s was evaluated by measuring the volume of NiO thin films deposited at room temperature since the re-evaporation rate is negligible at that temperature condition. The other experimental conditions such as the repetition rate, the growth time, and the cooling time after the nanowire growth were set to be 10 Hz and 60 and 30 min, respectively. The X-ray diffraction (XRD, Philips), the 30 kV field emission scanning electron microscopy (FESEM, JEOL JEM-7001F), and the 300 kV transmission electron microscopy (TEM, JEOL JEM-3000F) equipped with energy dispersive X-ray spectroscopy (EDS), and the 200 kV scanning transmission electron microscopy (STEM, JEOL JEM-ARM200F), were utilized to evaluate the crystal structure, the morphology, and the composition of fabricated oxide nanowires. The electrical transport measurement of a NiO nanowire was conducted in the form of a single oxide nanowire device, which was constructed onto the SiO_2/Si substrate by the 30 kV electron beam lithography technique.[44] For the electrical contact, a Pt electrode was sputtered via the RF magnetron sputtering at 50 W in Ar 1 Pa. The electrical transport measurement was carried out at room temperature in atmospheric conditions.

3. RESULTS AND DISCUSSION

First, we characterize the fabricated NiO nanowires, and then discuss the microscopic VLS process of NiO nanowires in terms of "material flux window" concept.[42] Figure 1a shows the typical FESEM images of fabricated NiO nanowires grown on a MgO(100) single crystal substrate. The growth temperature, Ni metal flux, and oxygen partial pressure were 850 °C, 1.8 × 10^{18} atoms/cm^2 s, and 10^{-3} Pa, respectively. The fabricated NiO nanowires grow perpendicular to the substrate due to the small lattice mismatch between MgO and NiO (∼0.95%), similar to

DOI: 10.1021/acsami.6b09761
ACS Appl. Mater. Interfaces 2016, 8, 27892−27899

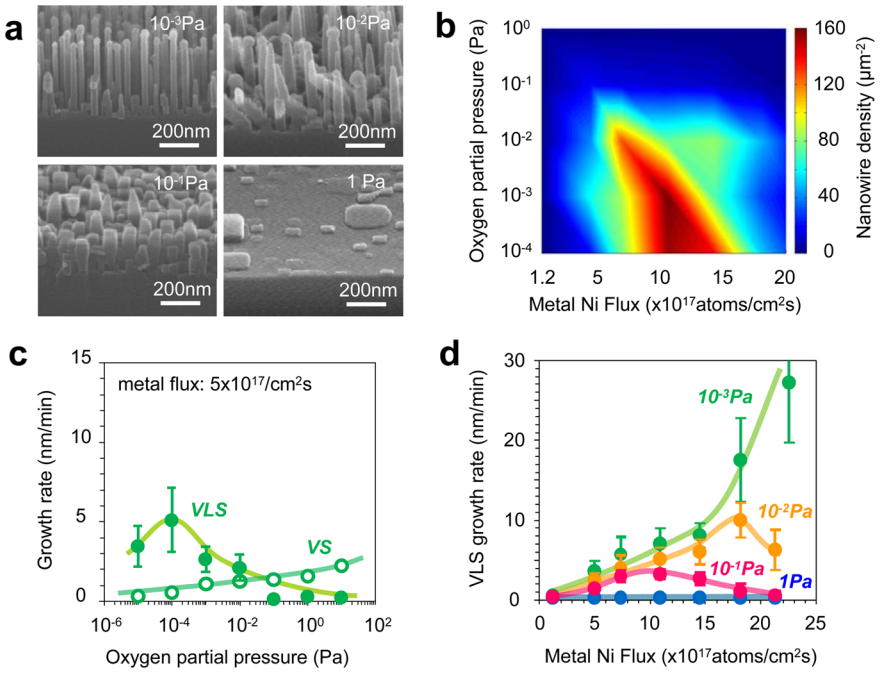

Figure 2. (a) SEM images of NiO nanowires when varying the vapor flux (oxygen partial pressure 10^{-3} Pa^{-1} Pa). (b) Nanowire density mapping as functions of both Ni flux and oxygen partial pressure, indicating the critical role of the vapor flux on the VLS growth of oxide nanowires. (c) The growth rate of NiO nanowires (VLS growth) and NiO films (VS growth) as functions of oxygen partial pressure. The Ni flux for part c was 5×10^{17} atoms/cm^2 s. (d) VLS nanowire growth rate of NiO nanowires as a function of Ni flux for various oxygen partial pressure conditions. The error bars show the standard deviation. Parts c and d show the fitted lines for experimental data.

NiO epitaxial films on MgO(100) substrate.[45] Figure 1b shows the TEM images of a NiO nanowire. The nanowire diameters ranged from 20 to 70 nm. The preferential [100] growth direction, the single crystallinity, and the cubic structure (lattice constant 4.17 Å) of the NiO nanowires were confirmed by the high resolution TEM image and the selective area electron diffraction (SAED) pattern. As seen in Figure 1b, the spherical shaped catalyst exists at the tip of NiO nanowire. As shown in Figure 1c, the EDS spectra data measured near the catalyst and at the nanowire body reveal that the catalyst and the nanowire are mainly composed of Au and NiO, respectively. The presence of Au catalyst at the tip of the nanowires suggests the occurrence of the VLS process for the present NiO nanowires.[46] Figure 1d shows the XRD pattern of NiO nanowires. XRD data only shows the NiO(002) related peaks, and any other peaks are not observed, which is consistent with the results of TEM-SAED analysis. To further confirm the occurrence of the VLS process for the present NiO nanowires, we performed the spatial patterning of Au catalysts on the substrate because NiO nanowires should grow only at the spatial positions where the Au catalysts are patterned on the basis of the VLS process. Figure 1e shows the SEM images of fabricated NiO nanowires when the Au catalysts are spatially patterned. As can be seen, the fabricated NiO nanowires grew only where the Au catalysts were patterned. Note that the scaling limitation, the density, and the size of the present spatial patterning depend on the spatial resolution of e-beam lithography, which is around 50 nm in our system, although better spatial resolution can be achievable by using a more advanced e-beam lithography system. Thus, these results highlight that the fabricated nanowires are single crystalline NiO via the VLS process with Au catalysts. It should be noted that these successful NiO nanowires could be fabricated only when we strictly controlled the vapor fluxes (metal and oxygen), as explained in the following discussion.

The importance of vapor flux for a VLS nanowire growth process has been proposed by using molecular dynamics simulation, which suggests the presence of a so-called "material flux window" where the nucleation preferentially occurs only at the liquid−solid (LS) interface.[42,47,48] The presence of such a material flux window was experimentally validated for the VLS process for metal oxide nanowires.[42,43] Within the framework of this concept, the size of the critical nucleus at the LS interface is smaller than that at the vapor−solid (VS) interface due to the surface energy gain by the surrounding liquid catalyst atoms, resulting in the preferential crystal growth only at the LS interface. Since the nucleation rate of the critical nucleus depends on the partial pressure of vapor, i.e., vapor flux, controlling the vapor flux is crucial for the VLS nanowire growth process.[42,43,49−51] Since both metal and oxygen are components of metal oxides, it is interesting to investigate the effect of each vapor flux, including Ni metal and oxygen fluxes, on the VLS process. By utilizing the present PLD deposition technique, it is possible to control individually the Ni metal flux and oxygen flux with other constant experimental conditions by altering the laser power and the target-to-substrate distance for the ablation of the Ni metal target and the oxygen partial pressure in the vacuum chamber.

Figure 2a shows the typical SEM images of fabricated NiO nanowires when varying the vapor flux (oxygen). The Ni metal flux was kept at 1.8×10^{18} atoms/cm^2 s, and the substrate temperature was 850 °C. As seen in the figure, the vapor flux strongly affects the shape of fabricated NiO nanowires. With an increase in the vapor flux, the NiO nanowire shape tends to be tapered and the VS film growth tends to be dominant rather than the VLS nanowire growth. For the highest vapor flux, the nanowire shapes are no longer observable, and only film

DOI: 10.1021/acsami.6b09761
ACS Appl. Mater. Interfaces 2016, 8, 27892−27899

structures are formed. To more quantitatively study the effect of vapor fluxes, we measured the nanowire density values from the SEM data. Figure 2b shows the NiO nanowire density data when varying Ni metal flux and oxygen flux (oxygen partial pressure). The NiO nanowires were grown at the constant temperature (850 °C). As can be seen, NiO nanowires can be grown within a rather limited flux range. For example, NiO nanowires were grown precisely only within the Ni metal fluxes, ranging from 5×10^{17} to 1.8×10^{18} atoms/cm^2 s in the constant oxygen partial pressure of 10^{-3} Pa. Thus, the VLS process of NiO nanowires requires the strict control of vapor fluxes including both Ni metal flux and oxygen partial pressures. This trend is consistent with the concept based on the "material flux window" of VLS process.[42]

To further examine the effect of vapor fluxes, we measured the growth rate of NiO nanowires from the cross-sectional SEM data. Figure 2c shows the growth rate of NiO nanowires (LS growth) and NiO films (VS growth) as a function of oxygen partial pressure. The NiO nanowires were grown at 850 °C with the constant Ni metal flux of 5×10^{17} atoms/cm^2 s. As can be seen, the growth rate of NiO nanowires via the VLS process showed the maximum at the oxygen partial pressure of 10^{-4} Pa. On the other hand, the growth rate of VS films monotonically increased with an increase in the oxygen partial pressure nearly above the oxygen partial pressure of 10^{-4} Pa, at which the growth rate of NiO nanowires showed the maximum. Clearly, the occurrence of the VS film growth hinders the VLS process of nanowires with variation in the oxygen partial pressure. Figure 2d shows the growth rate of NiO nanowires when varying only the Ni metal flux. The NiO nanowires were grown at constant temperature (850 °C), and various oxygen partial pressures ranged from 10^{-3} to 1 Pa. For the oxygen partial pressures of 10^{-2} and 10^{-1} Pa, the growth rate of NiO nanowires showed the maximum at a certain Ni metal flux (ca. 1.8×10^{18} atoms/cm^2 s for 10^{-2} Pa, ca. 1.1×10^{18} atoms/cm^2 s for 10^{-1} Pa). In the case of the oxygen partial pressure of 1 Pa, any nanowire structures were not observable, and only film structures appeared even with varying the Ni metal flux. Similar to the experimental trend upon varying the oxygen partial pressure (Figure 2c), the VLS nanowire growth rate tends to decrease when the VS film growth tends to be dominant when increasing the Ni metal flux. Thus, these results highlight that precisely manipulating the vapor fluxes including Ni metal and oxygen fluxes is essential to fabricate NiO nanowires via the VLS process. In other words, tailoring the nucleation at two interfaces (LS and VS interfaces) via controlling the vapor flux is a key process to accomplish the VLS process of NiO nanowires.

On the basis of the above implications, we further extend the concept to reduce the growth temperature of the VLS process for NiO nanowires since the relatively high growth temperature for the VLS process has limited the application range. Within the framework of the VLS process, the growth temperature must be high enough for catalysts to be in a liquid state. However, recent studies reveal that there is another growth process, the so-called vapor−solid−solid (VSS), when the growth temperature tends to be low.[52] In addition, the growth temperature should be also high enough for the nucleation at an LS interface but not for the nucleation at a VS interface. On the basis of the above concept for material vapor fluxes, it might be possible to reduce the growth temperature of the VLS process via controlling the vapor fluxes, since the nucleation rate at the interface is determined by supersaturation, defined as the difference between the vapor pressure and the saturated vapor pressure of target materials. The important point here is that the saturated vapor pressure shows strong temperature dependence, as shown in Figure 3. In general, the lower the

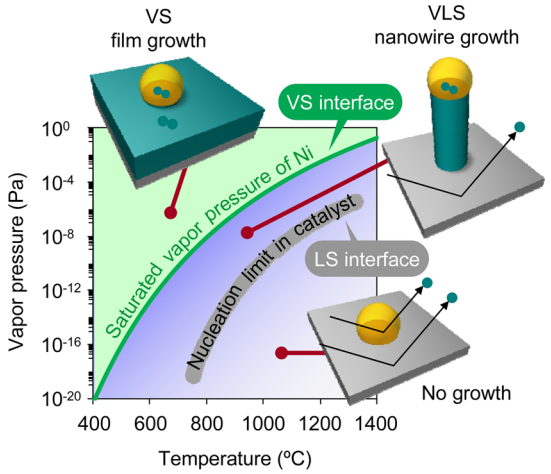

Figure 3. Thermodynamic phase diagram for the Ni nucleation at the LS and VS interface. When the vapor pressure is lower than that of the nucleation limit in catalyst, all Ni vapor is re-evaporated, and no nucleation occurs both at LS and VS interfaces. On the other hand, when the vapor pressure is higher than the saturated vapor pressure, the nucleation occurs both at LS and VS interfaces. Controlling the vapor pressure higher than the nucleation limit and lower than the saturated vapor pressure promotes the nucleation only at the LS interface, resulting in nanowires. When the temperature is reduced, appropriate vapor pressure for nanowire growth is varied. Therefore, precise control of vapor pressure is crucial for fabricating the nanowire at lower temperature.

temperature is, the lower the saturated vapor pressure is.[41] As illustrated in Figure 3, it should be possible to reduce the growth temperature of the VLS process by decreasing the supplied vapor fluxes.

Figure 4a shows the FESEM images of NiO nanowires with varying the growth temperature. In this experiment, the Ni flux was controlled to be as low as 7×10^{17} atoms/cm^2 s, and the oxygen partial pressure was fixed to be 10^{-3} Pa. Note that the NiO nanowire growth was not observable below 800 °C under the Ni flux condition of 2.3×10^{18} atoms/cm^2 s. Clearly, nanowire growth was observable even at 550 °C, which is much lower than any growth temperatures so far reported.[27,28] Thus, we successfully reduced the growth temperature of the VLS process for NiO nanowires by controlling the vapor flux based on the proposed concept. Figure 4b shows the temperature dependence on the growth rate of NiO nanowires. Below 700 °C, the growth rate increases with increasing the growth temperature, and above 700 °C the growth rates decreases. The trend below 700 °C can be understood in terms of the change of nucleation rate for the VS growth accompanied with the change of the saturated vapor pressure. In fact, the size of NiO nanowires tended to be larger at the lower growth temperature, indicating the increase of VS growth at the sidewall of NiO nanowires. However, the trend of the growth rate over 700 °C was completely opposite to the aforementioned situation. We found that this behavior can be understood by taking into account the competitive collection of supplied vapor species between adjacent nanowires. When we increased the growth temperature over 700 °C, the nanowire density greatly

DOI: 10.1021/acsami.6b09761
ACS Appl. Mater. Interfaces 2016, 8, 27892−27899

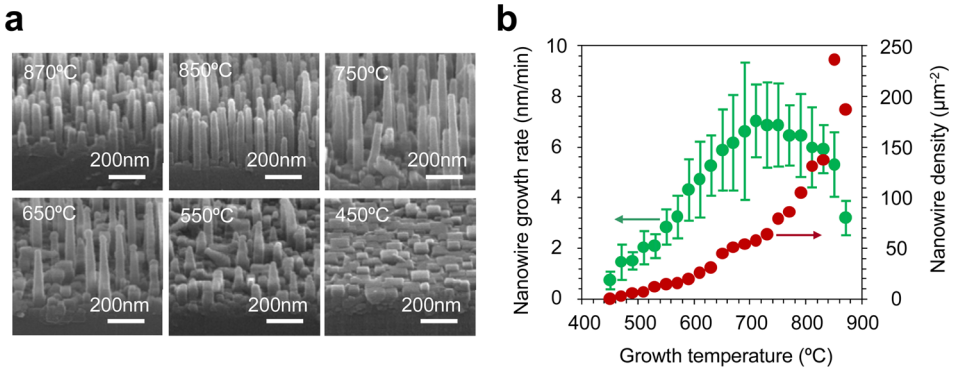

Figure 4. (a) FESEM images of NiO nanowires grown at various temperature conditions. The Ni flux and the oxygen partial pressure were 7×10^{17} atoms/cm^2 s and 10^{-3} Pa, respectively. (b) Temperature dependence on the growth rate and the density of NiO nanowires. The error bars show the standard deviation.

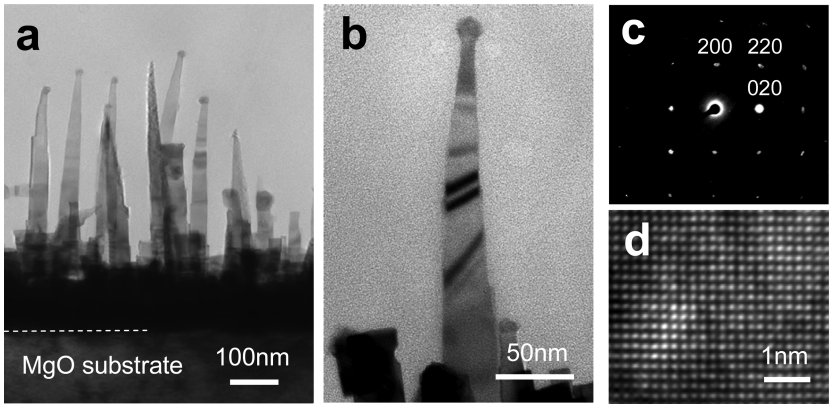

Figure 5. Cross-sectional TEM images of NiO nanowires grown at 620 °C: (a) overview, (b) magnified single nanowire, (c) SAED pattern, and (d) high resolution image. These data indicate the single crystal nature of NiO nanowires.

increased as shown in Figure 4b; i.e., the internanowire distance decreased. The decrease of internanowire distance causes the competitive collection of supplied vapor species between adjacent nanowires. The similar phenomenon was seen in MgO nanowire growth as reported by Annop et al.[53] As such, the variation of the competitive collection and the VS nucleation rate might coexist at the temperature condition over 700 °C. Note that the decrease of nanowire density with decreasing the growth temperature might be related to the solidification of Au metal catalyst. Since the melting point of bulk Au is 1064 °C and the eutectic point of Au−Ni is 955 °C (for 82:18 of Au:Ni ratio), the temperature condition of 600 °C might be low enough to solidify the Au catalyst. Once the metal catalyst solidifies, the growth mechanism of oxide nanowires relies on the VSS growth.[52] This might be another reason why the growth rate decreases below 700 °C. Thus, there might be the competition of VSS and VLS growth mechanisms in the current NiO nanowire growth. The VSS contribution tends to be dominant as the growth temperature decreases. On the other hand, as the growth temperature increases, the VLS contribution might be enhanced. Since the phase states of nanoscale metal catalysts somehow differ from those of bulk materials, it is necessary to experimentally observe the phase state of nanoscale metal catalysts when varying the growth temperature, for example, by using an in situ TEM method or an in situ X-ray method. Although this is a fascinating issue for future work, this is beyond our current scope of this work. To study the crystallinity of low temperature grown NiO nanowires, we performed TEM observations. Figure 5 shows the cross-sectional TEM images of NiO nanowires grown at 620 °C. Although there are slight tapering and the VS film underneath the NiO nanowires, the single crystalline nature of NiO nanowires was maintained as clearly seen in the magnified TEM image and the SAED pattern.

Finally, we show the device application of fabricated single crystalline NiO nanowires. Figure 6a shows the FESEM image of a NiO nanowire device in contact with Pt electrodes. The device was composed of a single NiO nanowire. The gap size between the Pt electrodes was 200 nm. Figure 6b shows the typical current−voltage (I−V) characteristics of the NiO nanowire device. The current compliance of 10^{-9} A was applied to prevent an irreversible electrical breakdown of the device. The measurement was carried out at room temperature in atmospheric conditions. As seen in the I−V curve, the device clearly showed a nonvolatile memory switching.[7−10] Note that the operation current of NiO nanowire device ($<10^{-9}$ A) was extremely small compared with that of conventional NiO film devices ($\sim 10^{-4}$−10^{-2} A).[7,54,55] This is interpreted in terms of the conduction within the small cross-sectional area of NiO nanowire device (ca. 2×10^3 nm^2), and this interesting feature is beneficial for low power consumption of the NiO nanowire-based electronic device applications. Here we analyze the electrical transport of NiO nanowires during the nonvolatile memory switching. Figure 6c shows the ON state resistances as a function of current density. For this measurement, the compliance currents were varied from 1×10^{-10} to 5×10^{-8} A.

DOI: 10.1021/acsami.6b09761
ACS Appl. Mater. Interfaces 2016, 8, 27892−27899

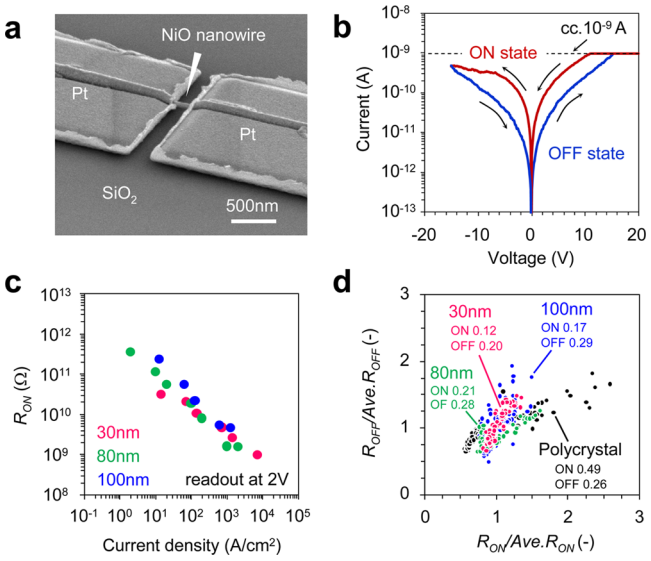

Figure 6. (a) FESEM image of NiO nanowire device. A single NiO nanowire was bridged between Pt electrodes. The gap size was 200 nm. (b) *I*−*V* curves of the NiO nanowire device measured at room temperature in air condition. The compliance current (cc.) of 10^{-9} A was applied to prevent the destructive electric breakdown. (c) ON state resistances as a function of current density for various sized NiO nanowires (30 nm, 80 nm, 100 nm). Readout voltage is 2 V. (d) The distribution of ON and OFF state resistances for various sized NiO nanowires. The data is taken from 100 *I*−*V* curves. For the comparison, the data from the polycrystal formed NiO nanobeam (diameter of 100 nm) is also shown. The standard deviation for both R_{ON}/AveR_{ON} and R_{OFF}/AveR_{OFF} is noted, which clearly shows the small distribution of ON and OFF resistance states in single crystalline NiO nanowire devices.

The resistances were measured at 2 V. As seen in Figure 6c, the electrical conductions of NiO nanowire devices are uniformly distributed into nanowires. In addition, the switching stability of the present single crystalline NiO nanowires is superior to other NiO nanostructure memristors, as shown in Figure 6d. Figure 6d shows the statistical distributions of ON state resistance and OFF state resistance, which are critical issues in industrial applications of nonvolatile memory devices. For comparison, data of polycrystalline NiO nanomemristors are shown. As can be seen, the statistical variation of single crystalline NiO nanowires, especially the small diameter (30 nm) NiO nanowires, is much smaller than the others. Although the exact mechanisms in the current NiO nanowire memristors should be further examined, the present experimental results highlight the importance of single crystallinity on the nanoscale memristive switching. The absence of grain boundaries seems to be responsible for the observed memristive properties of single crystalline NiO nanowires superior to polycrystalline nanowires. This effect of single crystalline nanostructures suppresses the variation of ON or OFF state resistances via limiting the conducting path in nanoscale.[38,39] Thus, the fabricated single crystalline NiO nanowires offer an opportunity to develop novel functional nanodevices.

4. CONCLUSION

In conclusion, we demonstrated a rational strategy to fabricate single crystalline NiO nanowires via a vapor−liquid−solid (VLS) route, which essentially allows us to tailor the diameter, the spatial position, and the heterostructures. Our strategy is based on the suppression of the vapor−solid (VS) nucleation at the substrate surface, which promotes the crystal growth of nanowires only at the liquid−solid (LS) interface. Manipulating the supplied material fluxes (oxygen and metal) and the growth temperature enables us to enhance the nucleation only at the LS interface. Furthermore, this strategy allows us to reduce the growth temperature of single crystalline NiO nanowires via the VLS route down to 550 °C, which is the lowest growth temperature so far reported. In addition, the fabricated single crystalline NiO nanowires exhibited the superior memristive properties.

AUTHOR INFORMATION

Corresponding Author

*E-mail: yanagida@cm.kyushu-u.ac.jp. Phone: +81-92-583-8829. Fax: +81-92-583-8820.

Notes

The authors declare no competing financial interest.

ACKNOWLEDGMENTS

This study was supported by CREST and Grant-in-Aid for Young Scientists (A) (No. 26706005) and ImPACT. K.N. was supported by Grant-in-Aid for Challenging Exploratory Research (No. 24651138). This work was performed under the Cooperative Research Program of "Network Joint Research Center for Materials and Devices".

REFERENCES

(1) Sato, H.; Minami, T.; Takata, S.; Yamada, T. Transparent conducting p-type NiO thin films prepared by magnetron sputtering. *Thin Solid Films* **1993**, *236*, 27−31.

(2) Sugiyama, I.; Shibata, N.; Wang, Z.; Kobayashi, S.; Yamamoto, T.; Ikuhara, Y. Ferromagnetic dislocations in antiferromagnetic NiO. *Nat. Nanotechnol.* **2013**, *8*, 266−270.

(3) Zhou, S.; Yin, H.; Schwartz, V.; Wu, Z.; Mullins, D.; Eichhorn, B.; Overbury, S. H.; Dai, S. In situ Phase Separation of NiAu Alloy Nanoparticles for Preparing Highly Active Au/NiO CO Oxidation Catalysts. *ChemPhysChem* **2008**, *9*, 2475−2479.

(4) Rebello, A.; Adeyeye, A. O. Robust electric-field tunable opto-electrical behavior in Pt-NiO-Pt planar structures. *Sci. Rep.* **2016**, *6*, 28007.

(5) Kim, S.-I.; Lee, J.-S.; Ahn, H.-J.; Song, H.-K.; Jang, J.-H. Facile Route to an Efficient NiO Supercapacitor with a Three-Dimensional Nanonetwork Morphology. *ACS Appl. Mater. Interfaces* **2013**, *5*, 1596−1603.

(6) Ci, S.; Wen, Z.; Qian, Y.; Mao, S.; Cui, S.; Chen, J. NiO-Microflower Formed by Nanowire-weaving Nanosheets with Interconnected Ni-network Decoration as Supercapacitor Electrode. *Sci. Rep.* **2015**, *5*, 11919.

(7) Ahn, S.-E.; Lee, M.-J.; Park, Y.; Kang, B. S.; Lee, C. B.; Kim, K. H.; Seo, S.; Suh, D.-S.; Kim, D.-C.; Hur, J.; Xianyu, W.; Stefanovich, G.; Yin, H.; Yoo, I.-K.; Lee, J.-H.; Park, J.-B.; Baek, I.-G.; Park, B. H. Write Current Reduction in Transition Metal Oxide Based Resistance Change Memory. *Adv. Mater.* **2008**, *20*, 924−928.

(8) Oka, K.; Yanagida, T.; Nagashima, K.; Tanaka, H.; Kawai, T. Nonvolatile Bipolar Resistive Memory Switching in Single Crystalline NiO Heterostructured Nanowires. *J. Am. Chem. Soc.* **2009**, *131*, 3434−3435.

(9) Oka, K.; Yanagida, T.; Nagashima, K.; Kawai, T.; Kim, J.-S.; Park, B. H. Resistive-Switching Memory Effects of NiO Nanowire/Metal Junctions. *J. Am. Chem. Soc.* **2010**, *132*, 6634−6635.

(10) Oka, K.; Yanagida, T.; Nagashima, K.; Kanai, M.; Kawai, T.; Kim, J.-S.; Park, B. H. Spatial Nonuniformity in Resistive-Switching Memory Effect of NiO. *J. Am. Chem. Soc.* **2011**, *133*, 12482−12485.

(11) Liu, H.; Wang, G.; Liu, J.; Qiao, S.; Ahn, H. Highly ordered mesoporous NiO anode material for lithium ion batteries with an

DOI: 10.1021/acsami.6b09761
ACS Appl. Mater. Interfaces 2016, 8, 27892−27899

excellent electrochemical performance. *J. Mater. Chem.* **2011**, *21*, 3046−3052.
(12) Sun, Y.-K.; Chen, Z.; Noh, H.-J.; Lee, D.-J.; Jung, H.-G.; Ren, Y.; Wang, S.; Yoon, C. S.; Myung, S.-T.; Amine, K. Nanostructred high-energy cathode materials for advanced lithium batteries. *Nat. Mater.* **2012**, *11*, 942−947.
(13) Farré, Y.; Zhang, L.; Pellegrin, Y.; Planchat, A.; Blart, E.; Boujtita, M.; Hammarström, L.; Jacquemin, D.; Odobel, F. Second Generation of Diketopyrrolopyrrole Dyes for NiO-Based Dye-Sensitized Solar Cells. *J. Phys. Chem. C* **2016**, *120*, 7923−7940.
(14) You, J.; Meng, L.; Song, T.-B.; Guo, T.-F.; Yang, Y.; Chang, W.-H.; Hong, Z.; Chen, H.; Zhou, H.; Chen, Q.; Liu, Y.; De Marco, N.; Yang, Y. Improved air stability of perovskite solar cells via solution-processed metal oxide transport layers. *Nat. Nanotechnol.* **2016**, *11*, 75−81.
(15) Oka, K.; Yanagida, T.; Nagashima, K.; Kanai, M.; Xu, B.; Park, B. H.; Katayama-Yoshida, H.; Kawai, T. Dual Defects of Cation and Anion in Memristive Nonvolatile Memory of Metal Oxides. *J. Am. Chem. Soc.* **2012**, *134*, 2535−2538.
(16) Oka, K.; Yanagida, T.; Nagashima, K.; Tanaka, H.; Seki, S.; Honsho, Y.; Ishimaru, M.; Hirata, A.; Kawai, T. Specific surface effect on transport properties of NiO/MgO heterostructured nanowires. *Appl. Phys. Lett.* **2009**, *95*, 133110.
(17) Marei, N. N.; Nassar, N. N.; Vitale, G. The effect of the nanosize on surface properties of NiO nanoparticles for the adsorption of Quinolin-65. *Phys. Chem. Chem. Phys.* **2016**, *18*, 6839−6849.
(18) Zhang, Z.; Zhao, Y.; Zhu, M. NiO films consisting of vertically aligned cone-shaped NiO rods. *Appl. Phys. Lett.* **2006**, *88*, 033101.
(19) Pang, H.; Lu, Q.; Zhang, Y.; Li, Y.; Gao, F. Selective synthesis of nickel oxide nanowires and length effect on their electrochemical properties. *Nanoscale* **2010**, *2*, 920−922.
(20) Patil, R. A.; Devan, R. S.; Lin, J.-H.; Liou, Y.; Ma, Y.-R. An efficient methodology for measurement of the average electrical properties of single one-dimensional NiO nanorods. *Sci. Rep.* **2013**, *3*, 3070.
(21) Liu, C.; Li, C.; Ahmed, K.; Mutlu, Z.; Ozkan, C. S.; Ozkan, M. Template Free and Binderless NiO Nanowire Foam for Li-ion Battery Anodes with Long Cycle Life and Ultrahigh Rate Capability. *Sci. Rep.* **2016**, *6*, 29183.
(22) Mintz, T. S.; Bhargava, Y. V.; Thorne, S. A.; Chopdekar, R.; Radmilovic, V.; Suzuki, Y.; Devine, T. M. Electrochemical Synthesis of Functionalized Nickel Oxide Nanowires. *Electrochem. Solid-State Lett.* **2005**, *8*, D26−D30.
(23) Kim, S. I.; Lee, J. H.; Chang, Y. W.; Hwang, S. S.; Yoo, K.-H. Reversible resistive switching behaviors in NiO nanowires. *Appl. Phys. Lett.* **2008**, *93*, 033503.
(24) Matsubara, K.; Huang, S.; Iwamoto, M.; Pan, W. Enhanced conductivity and gating effect of p-type Li-doped NiO nanowires. *Nanoscale* **2014**, *6*, 688−692.
(25) Xu, C.; Xu, G.; Wang, G. Preparation and characterization of NiO nanorods by thermal decomposition of NiC_2O_4 precursor. *J. Mater. Sci.* **2003**, *38*, 779−782.
(26) Lin, Y.; Xie, T.; Cheng, B.; Geng, B.; Zhang, L. Ordered nickel oxide nanowire arrays and their optical absorption properties. *Chem. Phys. Lett.* **2003**, *380*, 521−525.
(27) Kaur, N.; Comini, E.; Zappa, D.; Poli, N.; Sberveglieri, G. Nickel oxide nanowires: vapor liquid solid synthesis and integration into a gas sensing device. *Nanotechnology* **2016**, *27*, 205701.
(28) Kaur, N.; Comini, E.; Poli, N.; Zappa, D.; Sberveglieri, G. Nickel oxide nanowires growth by VLS technique for gas sensing application. *Procedia Eng.* **2015**, *120*, 760−763.
(29) Wu, Z. Y.; Liu, C. M.; Guo, L.; Hu, R.; Abbas, M. I.; Hu, T. D.; Xu, H. B. Structural Characterization of Nickel Oxide Nanowires by X-ray Absorption Near-Edge Structure Spectroscopy. *J. Phys. Chem. B* **2005**, *109*, 2512−2515.
(30) Wu, L.; Wu, Y.; Wei, H.; Shi, Y.; Hu, C. Synthesis and characteristics of NiO nanowire by a solution method. *Mater. Lett.* **2004**, *58*, 2700−2703.
(31) Wei, Z. P.; Arredondo, M.; Peng, H. Y.; Zhang, Z.; Guo, D. L.; Xing, G. Z.; Li, Y. F.; Wong, L. M.; Wang, S. J.; Valanoor, N.; Wu, T. A Template and Catalyst-Free Metal-Etching-Oxidation Method to Synthesize Aligned Oxide Nanowire Arrays: NiO as an Example. *ACS Nano* **2010**, *4*, 4785−4791.
(32) Nagashima, K.; Yanagida, T.; Tanaka, H.; Kawai, T. Epitaxial growth of MgO nanowires by pulsed laser deposition. *J. Appl. Phys.* **2007**, *101*, 124304.
(33) Yanagida, T.; Nagashima, K.; Tanaka, H.; Kawai, T. Mechanism of catalyst diffusion on magnesium oxide nanowire growth. *Appl. Phys. Lett.* **2007**, *91*, 061502.
(34) Yanagida, T.; Nagashima, K.; Tanaka, H.; Kawai, T. Mechanism of critical catalyst size effect on MgO nanowire growth by pulsed laser deposition. *J. Appl. Phys.* **2008**, *104*, 016101.
(35) Yanagida, T.; Marcu, A.; Matsui, H.; Nagashima, K.; Oka, K.; Yokota, K.; Taniguchi, M.; Kawai, T. Enhancement of Oxide VLS growth by Carbon on Substrate Surface. *J. Phys. Chem. C* **2008**, *112*, 18923−18926.
(36) Nagashima, K.; Yanagida, T.; Tanaka, H.; Seki, S.; Saeki, A.; Tagawa, S.; Kawai, T. Effect of the Heterointerface on Transport Properties of in Situ Formed MgO/Titanate Heterostructured Nanowires. *J. Am. Chem. Soc.* **2008**, *130*, 5378−5382.
(37) Marcu, A.; Yanagida, T.; Nagashima, K.; Oka, K.; Tanaka, H.; Kawai, T. Crucial role of interdiffusion on magnetic properties on in situ formed $MgO/Fe_{3-d}O_4$ heterostructured nanowires. *Appl. Phys. Lett.* **2008**, *92*, 173119.
(38) Nagashima, K.; Yanagida, T.; Oka, K.; Taniguchi, M.; Kawai, T.; Kim, J.-S.; Park, B. H. Resistive Switching Multistate Nonvolatile Memory Effects in a Single Cobalt Oxide Nanowire. *Nano Lett.* **2010**, *10*, 1359−1363.
(39) Nagashima, K.; Yanagida, T.; Oka, K.; Kanai, M.; Klamchuen, A.; Kim, J.-S.; Park, B. H.; Kawai, T. Intrinsic Mechanisms of Memristive Switching. *Nano Lett.* **2011**, *11*, 2114−2118.
(40) Meng, G.; Yanagida, T.; Nagashima, K.; Yoshida, H.; Kanai, M.; Klamchuen, A.; Zhuge, F. W.; He, Y.; Rahong, S.; Fang, X.; Takeda, S.; Kawai, T. Impact of Preferential Indium Nucleation on Electrical Conductivity of Vapor-Liquid-Solid Grown Indium-Tin Oxide Nanowires. *J. Am. Chem. Soc.* **2013**, *135*, 7033−7038.
(41) Lide, D. R. *CRC Handbook of Chemistry and Physics*, 84th ed.; Section 6 Fluid Properties; CRC Press, 2003.
(42) Klamchuen, A.; Suzuki, M.; Nagashima, K.; Yoshida, H.; Kanai, M.; Zhuge, F. W.; He, Y.; Meng, G.; Kai, S.; Takeda, S.; Kawai, T.; Yanagida, T. Rational Concept for Designing Vapor-Liquid-Solid Growth of Single Crystalline Metal Oxide Nanowires. *Nano Lett.* **2015**, *15*, 6406−6412.
(43) Zhuge, F. W.; Yanagida, T.; Nagashima, K.; Yoshida, H.; Kanai, M.; Xu, B.; Klamchuen, A.; Meng, G.; He, Y.; Rahong, S.; Li, X.; Suzuki, M.; Kai, S.; Takeda, S.; Kawai, T. Fundamental Strategy for Creating VLS Grown TiO_2 Single Crystalline Nanowires. *J. Phys. Chem. C* **2012**, *116*, 24367−24372.
(44) Nagashima, K.; Yanagida, T.; Klamchuen, A.; Kanai, M.; Oka, K.; Seki, S.; Kawai, T. Interfacial effect on metal/oxide nanowire junctions. *Appl. Phys. Lett.* **2010**, *96*, 073110.
(45) Oka, K.; Yanagida, T.; Nagashima, K.; Tanaka, H.; Kawai, T. Growth atmosphere dependence of transport properties of NiO epitaxial thin films. *J. Appl. Phys.* **2008**, *104*, 013711.
(46) Wagner, R. S.; Ellis, W. C. VAPOR-LIQUID-SOLID MECHANISM OF SINGLE CRYSTAL GROWTH. *Appl. Phys. Lett.* **1964**, *4*, 89−90.
(47) Suzuki, M.; Hidaka, Y.; Yanagida, T.; Kanai, M.; Kawai, T.; Kai, S. Numerical study on the difference in mechanism between vapor-solid and vapor-liquid-solid solidification processes. *Phys. Rev. E* **2010**, *82*, 011605.
(48) Suzuki, M.; Hidaka, Y.; Yanagida, T.; Klamchuen, A.; Kanai, M.; Kawai, T.; Kai, S. Essential role of catalyst in vapor-liquid-solid growth of compounds. *Phys. Rev. E* **2011**, *83*, 061606.
(49) Marcu, A.; Yanagida, T.; Nagashima, K.; Tanaka, H.; Kawai, T. Effect of ablated particle flux on MgO nanowire growth by pulsed laser deposition. *J. Appl. Phys.* **2007**, *102*, 016102.

DOI: 10.1021/acsami.6b09761
ACS Appl. Mater. Interfaces 2016, 8, 27892−27899

(50) Nagashima, K.; Yanagida, T.; Oka, K.; Tanaka, H.; Kawai, T. Mechanism and control of sidewall growth and catalyst diffusion on oxide nanowire vapor-liquid-solid growth. *Appl. Phys. Lett.* **2008**, *93*, 153103.
(51) Klamchuen, A.; Yanagida, T.; Kanai, M.; Nagashima, K.; Oka, K.; Kawai, T.; Suzuki, M.; Hidaka, Y.; Kai, S. Role of surrounding oxygen on oxide nanowire growth. *Appl. Phys. Lett.* **2010**, *97*, 073114.
(52) Kodambaka, S.; Tersoff, J.; Reuter, M. C.; Ross, F. M. Germanium Nanowire Growth Below the Eutectic Temperature. *Science* **2007**, *316*, 729−732.
(53) Klamchuen, A.; Yanagida, T.; Kanai, M.; Nagashima, K.; Oka, K.; Rahong, S.; Gang, M.; Horprathum, M.; Suzuki, M.; Hidaka, Y.; Kai, S.; Kawai, T. Study on transport pathway in oxide nanowire growth by using spacing-controlled regular array. *Appl. Phys. Lett.* **2011**, *99*, 193105.
(54) Nagashima, K.; Yanagida, T.; Kanai, M.; Celano, U.; Rahong, S.; Meng, G.; Zhuge, F. W.; He, Y.; Park, B. H.; Kawai, T. Carrier type dependence on spatial asymmetry of unipolar resistive switching of metal oxides. *Appl. Phys. Lett.* **2013**, *103*, 173506.
(55) Yanagida, T.; Nagashima, K.; Oka, K.; Kanai, M.; Klamchuen, A.; Park, B. H.; Kawai, T. Scaling Effect on Unipolar and Bipolar Resistive Switching of Metal Oxides. *Sci. Rep.* **2013**, *3*, 1657.

DOI: 10.1021/acsami.6b09761
ACS Appl. Mater. Interfaces 2016, 8, 27892−27899